

Citation for published version:
Hamaza, S, Georgilas, I & Richardson, T 2019, Energy-Tank based Force Control for 3D Contour Following. in K Althoefer, J Konstantinova & K Zhang (eds), *Towards Autonomous Robotic Systems - 20th Annual Conference, TAROS 2019, Proceedings.* Lecture Notes in Computer Science (including subseries Lecture Notes in Artificial Intelligence and Lecture Notes in Bioinformatics), vol. 11649 LNAI, Springer Vival pp. 41-51, 20th Towards Autonomous Robotic Systems Conference, London, UK United Kingdom, 3/07/19. https://doi.org/10.1007/978-3-030-23807-0 4

DOI:

10.1007/978-3-030-23807-0 4

Publication date:

Document Version Peer reviewed version

Link to publication

This is a post-peer-review, pre-copyedit version of a conference article published in TAROS 2019: Towards Autonomous Robotic Systems. The final authenticated version is available online at: https://doi.org/10.1007/978-3-030-23807-0 4

University of Bath

Alternative formats

If you require this document in an alternative format, please contact: openaccess@bath.ac.uk

Copyright and moral rights for the publications made accessible in the public portal are retained by the authors and/or other copyright owners and it is a condition of accessing publications that users recognise and abide by the legal requirements associated with these rights.

Take down policy

If you believe that this document breaches copyright please contact us providing details, and we will remove access to the work immediately and investigate your claim.

Download date: 07. Mar. 2023



Citation for published version:
Hamaza, S, Georgilas, I & Richardson, T 2019, 'Energy-Tank based Force Control for 3D Contour Following' Paper presented at 20th Towards Autonomous Robotic Systems Conference, London, UK United Kingdom, 3/07/19 - 5/07/19, . https://doi.org/10.1007/978-3-030-23807-0_4

10.1007/978-3-030-23807-0_4

Publication date: 2019

Document Version Peer reviewed version

Link to publication

University of Bath

Copyright and moral rights for the publications made accessible in the public portal are retained by the authors and/or other copyright owners and it is a condition of accessing publications that users recognise and abide by the legal requirements associated with these rights.

Take down policy
If you believe that this document breaches copyright please contact us providing details, and we will remove access to the work immediately and investigate your claim.

Download date: 04. Jul. 2019

Energy-Tank based Force Control for 3D Contour Following

Salua Hamaza $^{1,3[0000-0001-5261-2680]},$ Ioannis Georgilas $^{2[0000-0001-8986-8102]},$ and Thomas Richardson $^{1,3[0000-0001-7767-452X]}$

- Bristol Robotics Laboratory, Bristol, BS16 1QY, UK http://www.brl.ac.uk/
- ² Dept. Mechanical Engineering, University of Bath, Bath, UK i.georgilas@bath.ac.uk
- Dept. Aerospace Engineering, University of Bristol, Bristol, UK {s.hamaza,thomas.richardson}@bristol.ac.uk

Abstract. Manipulation has been a major topic in robotics since its earlier developments. In the last few years, a new research area has focused in the introduction of manipulation capabilities on mobile robots. Several challenges are faced when mobile robots interact with unknown environments, for which inherent compliance is a key feature to achieve the intended outcome in a safe and robust way. This paper proposes a unified method of force control with energy-tank based methods to tackle 3D contour following. This method is tailored for manipulators that are designed for aerial applications, and addresses the interaction with unknown surfaces by also tackling the safety aspect, i.e. the response generated during contact loss.

Keywords: Manipulation · Mechatronics · Compliance · Control.

1 Introduction

Nowadays unmanned aerial vehicles (UAVs) are deployed for a variety of tasks that range from passive observation, e.g. inspection, environmental surveying, infrastructure monitoring, to contact-based applications such as transportation of objects [1, 15, 17], non-destructive testing [12] and simple maintenance tasks [16, 19]. The term *aerial manipulation* has been coined to describe this class of robots that are able to carry out manipulation tasks airborne by means of mechanical devices, i.e. manipulators, mounted on top of the flying platform.

The state-of-the-art in robotic manipulation from the past four decades has demonstrated that compliance is a key aspect [13, 20]. Standard manipulation using robotic arms has been augmented with compliance either via software with an active control, or through hardware with the introduction of mechanical elements that resemble a spring-damper system. Likewise, compliance is also a key feature in aerial manipulation thanks to the several advantages that it brings to the aerial system as a whole. Some of these advantages are energy absorbance in case of collision [2], force estimation and obstacle detection [24], and improved in-flight stability thanks to the dampening of perturbations [9, 10].

2 S. Hamaza et al.

In this paper we propose a passivity-based force controller tailored for aerial manipulation, using energy-tank based methods. Such approach is implemented for 3D contour following, and is particularly suited for aerial systems interacting with unknown structures. In fact, the combination of the force-tracking with inherent compliance of the energy-tank based method allows to safely interact with un-modeled environments. The envisioned aerial application for such contour following is to aid indoor navigation of UAVs, for example in a search and rescue scenario. Often UAVs are deployed to enter wrecked buildings after an earthquake or other natural calamities, having only to rely on visual sensing for indoor navigation due to the signal occlusion on GPS tracking. A more robust way to safely navigate and map such unknown environments would be to include tactile feedback to the aerial platform. Contour following is a useful property that aerial manipulators can exploit for example to detect crevices and doorways in which the UAV can fly into.

The proposed control approach is presented and then validated through experiments validating contouring capabilities on different 3D profiles. Experiments also address the case scenario of contact loss with the environment. Overall this approach achieves a good accuracy and shows great potential for its use on-board mobile robots.

1.1 Related Work

Interaction control strategies can be sub-categorised into direct and indirect force control. The direct approach achieves the force regulation of the end-effector by adopting an integral action on the force error. Such error is often generated by an outer force loop, hence an additional force feedback loop. On the other hand, indirect force control is based on impedance and compliance control where the output force is the result of an inner motion loop; without the explicit closure of a force feedback loop [22]. In the works presented in [3,4] a constrained-based approach that allows to selectively control force, impedance and position has been proposed. Moreover, hybrid position/force control gained popularity in the last two decades as it allows to work in force and motion sub-spaces that are complimentary to each other depending on the task specification. Despite the versatility of hybrid control, the major drawbacks associated with it are the need for an accurate modeling of the contact properties a-priori to reach a good performance, and the lack of robustness during contact-loss [18]. In [14] a variable-impedance control applied to an aerial platform is proposed, capable of adjusting the impedance of the multi-rotor and regulate the time-varying interaction forces. However this approach focuses on a time-varying force output for safe and robust compensation of disturbances in the environment rather than force-tracking and contouring. In this paper we propose a force control architecture that includes the concept of energy tanks [5,6] for aerial interaction applications in contour following. This approach is aimed for interaction airborne with 3D surfaces and accounts for the lack of prior knowledge of the environment, therefore avoiding pre-modeled variations in the force-tracking.

2 Modeling

2.1 Rigid Joint Dynamics

The equations of motion of a manipulation system with n rigid joints can be derived using the Newton-Euler approach:

$$\mathbf{M}(\mathbf{q})\ddot{\mathbf{q}} + \mathbf{C}(\mathbf{q}, \dot{\mathbf{q}})\dot{\mathbf{q}} + \mathbf{G}(\mathbf{q}) = \tau_m + \tau_{ext}$$
 (1)

where $\mathbf{M}(\mathbf{q}) \in \mathbb{R}^{n \times n}$ is the generalised mass matrix, matrix $\mathbf{C}(\mathbf{q}, \dot{\mathbf{q}}) \in \mathbb{R}^n$ represents the Coriolis and centrifugal terms, and $\mathbf{g}(\mathbf{q})$ comprises of all gravitational terms acting on the manipulator. On the right side of the equation, τ_m comprises the motor torque and the control input of the system, and τ_{ext} consists of all externally applied torques. Vectors $\mathbf{q}, \dot{\mathbf{q}}, \ddot{\mathbf{q}} \in \mathbb{R}^n$ represent the generalised coordinates of the manipulator and its time derivatives.

2.2 Flexible Joint Dynamics

For a robot with n flexible joints, i.e. an actuator that contains an elastic element such as series elastic actuator (SEA), the above equation is not sufficient to describe the dynamics of the inherent flexible transmission. Following the work proposed in [23], the equation of motion adapted for a flexible joint type of manipulator is:

$$\mathbf{M}(\mathbf{q})\ddot{\mathbf{q}} + \mathbf{C}(\mathbf{q}, \dot{\mathbf{q}})\dot{\mathbf{q}} + \mathbf{G}(\mathbf{q}) = \tau_{flex} + \tau_{ext}$$
 (2)

$$\mathbf{J}\ddot{\boldsymbol{\theta}} - \tau_{flex} = \tau_m \tag{3}$$

$$\tau_{flex} = \mathbf{K}(\boldsymbol{\theta} - \mathbf{q}) \tag{4}$$

where τ_{flex} represents the elastic joint torque, $\mathbf{J} \in \mathbb{R}^{n \times n}$ and $\mathbf{K} \in \mathbb{R}^{n \times n}$ are both diagonal positive definite matrices expressing the motor inertia and the joint stiffness respectively and $\boldsymbol{\theta}$ represents the motor position.

3 Control

3.1 Force Control Design

The proposed controller is designed for a generic n-DoF manipulator actuated by DC motors. These type of motors present a linear relationship between the input current and output torque, in accordance with the motors specifications. To achieve direct force-tracking on the end-effector, a current controller is implemented with a Proportional-Integral control law as follows:

$$\tau_m = J^T(\mathbf{q}) \left[K_T \left[k_p \left(c(t) - c_d(t) \right) + k_i \int_0^t \left(c(t) - c_d(t) \right) dt \right] \right]$$
 (5)

where τ_m is the output torque generated by the manipulator and linked to the output force; J^T is the transpose of the Jacobian matrix which only depends on the manipulator's configuration, i.e. the vector of generalised coordinates $\mathbf{q} \in \mathbb{R}^n$. The parameter K_T is the motor's torque-current constant, provided by the motor's manufacturer. k_p and k_i are the proportional and integral gains respectively, and c and c_d are the actual and desired current values.

S. Hamaza et al.

3.2 Energy Tank Design

Energy tank-based methods have frequently been used in tele-operated manipulation methods [7, 8, 21] and they have recently been applied to impedance controller with variable stiffness [6]. The role of the energy tank is to act as a storage element and minimise the energy dissipated by the controlled system. Such dissipated energy represents a *passivity threshold*, and the tank being its reservoir. Therefore, the presence of the tank allows to adjust the impedance of the system.

The variable $x_t(t) \in \mathbb{R}$ is the state associated with the tank. The tank energy is:

$$T(x_t) = \frac{1}{2}x_t^2\tag{6}$$

where $x_t(0) > 0$, and the dynamics are given by:

$$\begin{cases} \dot{x}_t = \frac{\beta}{x_t} \left(\dot{\tilde{x}}^T D_d \dot{\tilde{x}} \right) + u_T \\ \tilde{x}(t) = x(t) - x_d(t) \\ u_T = -w(t)^T \dot{\tilde{x}}_t \end{cases}$$
(7)

where \tilde{x} represents the state error, and β is defined as:

$$\beta = \begin{cases} 1 & \text{if } T \le T_{upper} \\ 0 & \text{otherwise} \end{cases}$$
 (8)

The term w(t) is the tank control input, β is a design parameters that enables the storage of dissipated energy as long as the total tank energy is less than an upper bound T_{upper} . Otherwise, the tank is disabled as β is zero, to avoid excessive storage. The product $(\dot{x}^T D_d \, \dot{x})$ represents the power dissipated. The extended motor dynamics of the system are described by:

$$\tau_m' = J^T(\mathbf{q}) \alpha \left[K_p(F_{ext} - F_{des}) + K_d(\dot{F}_{ext} - \dot{F}_{des}) + \dots \right]$$

$$\dots K_i \int_0^t (F_{ext} - F_{des})$$
(9)

where α is defined as:

$$\alpha = \begin{cases} 1 & \text{if } T \ge T_{lower} \\ 0 & \text{otherwise} \end{cases}$$
 (10)

where $T_{lower} > 0$ represents the lower bound below which the energy cannot be extracted by the tank, leading to $\alpha = 0$ and preventing singularities to occur.

3.3 Case Scenario: Contact Loss

Contact loss can be a recurring scenario during manipulation with an unmodeled environment, even more likely to occur if the interaction is performed on-board of a UAV. Aerial vehicles tend to be unstable in the proximity of obstacles, leading to disturbances



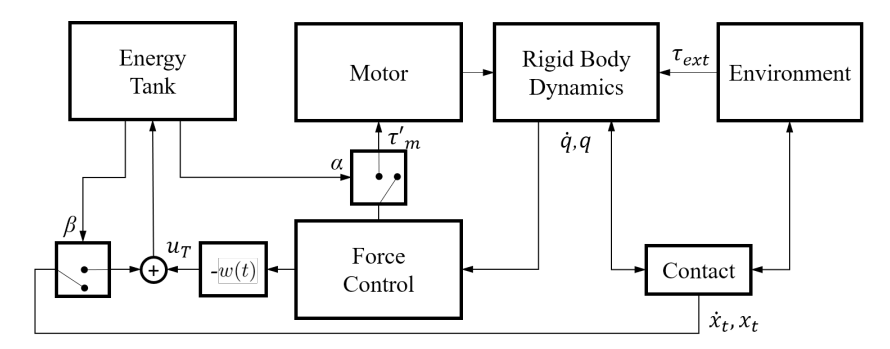


Fig. 1: Block diagram of the control architecture.

that often generate altitude loss and drifting. Therefore, it is essential that a manipulator intended for aerial applications is able to cope with contact loss, preventing it from executing unsafe motions. Typically, manipulators that solely operate with force-tracking would try to apply the desired force F_{des} regardless contact with the environment is established. The tank-based design brings an improvement to pure force-tracking as the output force is regulated until the tank energy is drained and the lower bound T_{lower} is reached. However, depending on the remaining energy in the tank, undesired substantial and rapid motion can still occur.

To address contact loss, we propose a port-based control architecture where the controller is switched on and off depending on the contact information sensed at the endeffector. This port-based model works by reading the end-effector states, i.e. position, velocity and current/force, and computing the overall kinetic and potential energy of the manipulator at any given time. During contact loss the output energy quickly reaches higher values as it is dependent on the square of the velocity $\dot{\mathbf{x}}_{\mathbf{t}}$. Once the saturation point is met, a signal is sent to the energy-tank control block that forces its drainage by setting $\beta=0$ (see Eq. (8)). As a result the controller output is set as zero. In Fig. 1 a control block diagram of the passivity-based force control via Energy-Tanks model is illustrated.

4 Manipulator Design

In the aerial manipulation state-of-the-art, a recurrent approach is to employ multi-DoF serial manipulators on top of UAVs, providing *n* additional DoFs to the overall aerial structure. Despite the dexterity that a higher-DoF manipulator offers in terms of tasks that can be accomplished, there are several drawbacks that come with it. The main problem with the presence of multiple actuators on a UAV is the increased payload that causes a shorter battery life and decreased manoeuvrability [11]. Another problem associated with high-DoF manipulators is the higher kinematics and control complexity, which often requires higher processing power and can drastically slow down computation time. In general, most aerial tasks may require limited manipulation capabilities as the exertion of a force on a surface for non-destructive-testing or inspection purposes. Such simple operations can be achieved with a simple 1-DoF manipulator oriented to-

6 S. Hamaza et al.

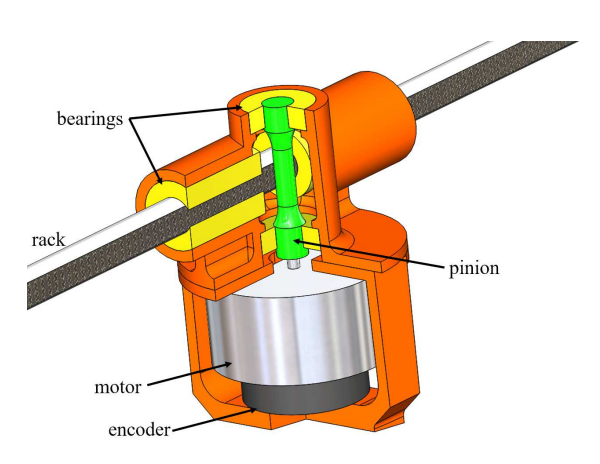


Fig. 2: Drawing of the manipulator's transmission mechanism. The pinion (in green) drives the motion of the toothed rack in a backdrivable way. The encoder measures the relative position of the motor shaft, therefore informing the system on the end-effector's relative position.

wards the contact surface. Despite its simplicity and limited dexterity, this approach provides a minimal, weight-efficient solution for force-driven tasks.

The proposed design consists of a single-DoF manipulator actuated by a prismatic joint. Amongst the improvements brought up from its previous version seen in [9] there is a more powerful on-board computer, i.e. Raspberry Pi 3 (1.4 GHz 64-bit quadcore ARM Cortex-A53 processor) with Wi-Fi connectivity and logging capabilities. On-board sensing is also integrated in the manipulator, in particular a rangefinder Teraranger One® based on Time-Of-Flight principle and an Maxon® MILE digital encoder on the slider joint that measures the end-effector relative position. Both sensors have a high sampling rate up to 1 kHz and allow for real-time feedback. A Maxon[®] DC motor actuates the prismatic joint via a pinion-rack transmission and it has its own dedicated motor board, namely a Maxon EPOS 2 24/3 Digital Controller. This controller board is particularly well-suited for real-time control as it provides a sampling rate of 10 kHz on the *current* output. The pinion-rack transmission is made out of lightweight, sturdy aluminium components. The mechanism housing is made out of 3D printed material and holds 4 bearings, 2 radial and 2 linear bearings respectively, within a crossshaped profile. The bearings allow to distress the motor shaft from any radial tension that might generate during the interaction. The overall weight on the manipulator, including the hardware, sensing and electronics is 450 g. A Computer-Aided-Drawing of the mechanical design is presented in Fig. 2 illustrating a detail of the transmission mechanism.

To minimise friction on the end-effector and guarantee a smooth contouring even on indentations that might be present on the target surface, a metal ball caster of 15 mm diameter is mounted at the tip. The ball caster is also ideal as it reduces the contact surface to a single point, therefore zeroing the moments of the external wrench τ_{ext} leading to pure force exchange F_{ext} .

5 Experiments

5.1 Experimental Setup

The setup used to validate the proposed control architecture includes the 1-DoF manipulator presented earlier mounted on a stationary base; a 6-axis force/torque sensor to measure the output force and the target surface that we aim to contour follow. The sensor chosen is the Robotiq FT 300 and, sampling at the rate of 100 Hz. The sensor data act as ground truth measurements rather than a feedback for the controller loop, in fact the estimated force on the end-effector is directly derived from the current information through the use of the torque constant K_T (see Section 3.1). Figure 3 illustrates a snapshot of the setup during the experiments with a close up on the 1-DoF manipulator in contact with the sensor.



Fig. 3: Experimental setup: 1-DoF manipulator equipped with a friction-less end-effector, exerting force over a 6-axis Force/Torque sensor.

5.2 Results

Several experiments are conducted to validate the proposed passivity-based force control with energy-tank. For each experiment, a different 3D profile with curvatures of different radius spanning from 1cm to 10 cm was contoured to validate the robustness of the control approach. The experiments aim to validate the ability to:

- 3D contour follow an unknown surface;
- establish a force pushing forwards whilst in contact;
- respond to an external input from the environment (τ_{ext}) in a compliant/ passive way:
- cease any force/motion as contact loss with the target is sensed;
- show the robustness of the controller by contouring differently shaped profiles.

In Fig. 4 the results of a single sample experiment are illustrated, with a focus on the force output generated on the surface (top figure) and the end-effector's position, velocity and current states (bottom figure). To understand the behaviour of the end-effector we can start by looking at the position profile (red line) for which the y-axis lays on the



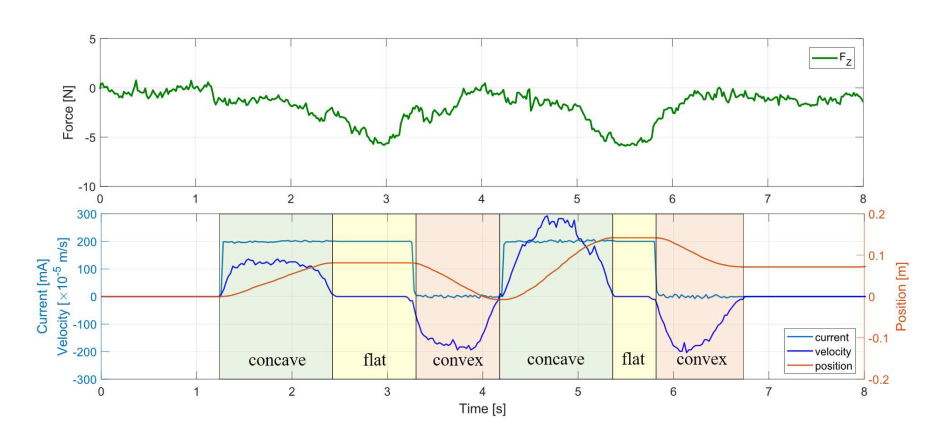


Fig. 4: 3D contour following experiment highlighting the force curve (top) and the end-effector's position, velocity and current states (bottom).

right side of the bottom plot. The manipulator starts at position 0 and moves forwards of about $0.1\,\mathrm{m}$ until it reaches a plateau, then goes backwards at about $t=3.3\,\mathrm{seconds}$. The velocity profile (blue line) for which the y-axis lays on the left side, is either positive, when motion forward is generated, or negative when the rack moves backwards. The zero in velocity always follows the position plateau: when the end-effector position is constant, its time derivative is zero. It can be noticed that during the position plateau, the force sensed on the Force/Torque sensor reaches 5 N (green line in the top figure). The presence of the plateau suggests that the target surface is flat (highlighted in the yellow areas), hence no motion is generated in either directions. Positive velocity suggests that the target profile is concave (green areas), viceversa negative velocity results from a convex profile (red areas).

The current profile is displayed as a light blue line in the same graph, with its y-axis on the left side of the figure along with the velocity profile. The current drives the rack at 200 mA and actively moves the end-effector towards the target. As the encoder senses an external force pushing the rack backwards, the *current* output is set as zero and the end-effector responds in a passive way. This occurs every time the manipulator is in contact with a convex profile, causing the end-effector to move backwards. As the targeted contour profile starts to flatten or becomes concave, the current input is set to positive again and the end-effector maintains contact with the surface. The transition between concavity and convexity acts as a trigger on the manipulator as the external wrench is no longer zero: $\tau_{ext} > 0$. In the figure, the phases of the task are highlighted within green, yellow and orange boxes as the manipulator contours a concave, flat or convex profile.

In Fig. 5 another sample experiment is illustrated. As seen above, the position, velocity and current curves are highlighted inside yellow, green and red boxes describing the flat, concave and convex profile respectively of the contoured structure. Additionally, this figure presents a purple area towards the end of the experiment that highlights the "contact loss" section. It is to be noted that the position curve starts at an initial



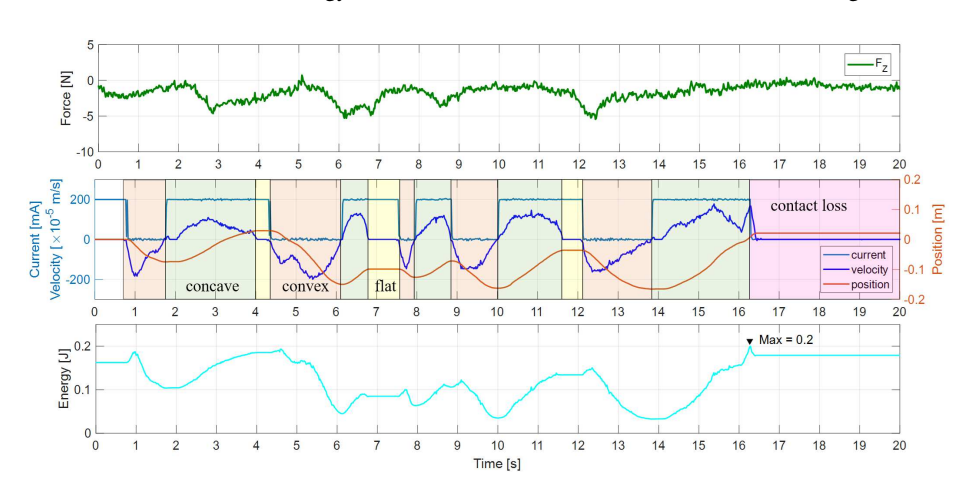


Fig. 5: Experiment demonstrating 3D contour following for longer periods. From top to bottom: force curve; position, velocity and current curves; and the tank energy curve.

value of 0 and this is just to characterise the start of the experiment, associated with a zero encoder value rather than a specific physical position of the manipulator.

The force curve in the top figure shows on average -2 N of force being exerted by the manipulator, with peaks up to -5 N. Towards the end of the experiment, at t=16.2s the manipulator experiences contact loss with the environment, as the target surface is purposely removed. As a consequence, the force output on the sensor goes to 0 N, while the manipulator's velocity spikes towards higher values, triggering the *no contact* condition. The energy value inside the virtual tank reaches its upper threshold, as illustrated in the bottom figure (cyan curve). Hence, the tank is instantaneously drained and both current and velocity values quickly move to zero. The effectiveness of the contact less condition can be seen in the position curve (red line) by looking at the displacement of the end-effector since the moment of the contact loss detection: the rack only displaces by 11 mm since the condition is met.

To conclude, the experiments showed a good accuracy in 3D contour following using a 1-DoF manipulator mounted on a stationary base. The experiments demonstrated that continuous contact was kept despite the irregularly shaped profiles and robust control was achieved throughout multiple trials. The ability to cope with contact loss was also demonstrated, as this is a key feature for a manipulator that could operate on mobile robots such as UAVs.

6 Conclusion

In this paper we propose the use of force control integrated with energy-tank based methods for contour following applications with 3D unknown surfaces. The addition of the virtual energy-tank allows to implement a more efficient passivity-based controller and is most suited when interacting with un-modeled environments. Such controller is validated on a single-DoF manipulator in several experiments and demonstrates the accuracy of the compliant interaction as well as its robustness with fast changing profiles.

10 S. Hamaza et al.

The specific *contact loss* scenario is also validated during the interaction showing fast response and minimal energy consumption. Overall this approach demonstrates great potential for its use on flying platforms for aerial manipulation applications.

Acknowledgements

This work is supported by the EPSRC Centre for Doctoral Training in Future Autonomous and Robotic Systems (FARSCOPE).

References

- Augugliaro, F., Lupashin, S., Hamer, M., Male, C., Hehn, M., Mueller, M.W., Willmann, J.S., Gramazio, F., Kohler, M., D'Andrea, R.: The flight assembled architecture installation: Cooperative construction with flying machines. Control Systems, IEEE 34(4), 46–64 (2014)
- 2. Bartelds, T., Capra, A., Hamaza, S., Stramigioli, S., Fumagalli, M.: Compliant aerial manipulators: Toward a new generation of aerial robotic workers. IEEE Robotics and Automation Letters pp. 477–483 (Jan 2016)
- Borghesan, G., De Schutter, J.: Constraint-based specification of hybrid position-impedanceforce tasks. In: Robotics and Automation (ICRA), 2014 IEEE International Conference on. pp. 2290–2296. IEEE (2014)
- De Schutter, J., De Laet, T., Rutgeerts, J., Decré, W., Smits, R., Aertbeliën, E., Claes, K., Bruyninckx, H.: Constraint-based task specification and estimation for sensor-based robot systems in the presence of geometric uncertainty. The International Journal of Robotics Research 26(5), 433–455 (2007)
- Ferraguti, F., Preda, N., Manurung, A., Bonfe, M., Lambercy, O., Gassert, R., Muradore, R., Fiorini, P., Secchi, C.: An energy tank-based interactive control architecture for autonomous and teleoperated robotic surgery. IEEE Transactions on Robotics 31(5), 1073–1088 (2015)
- 6. Ferraguti, F., Secchi, C., Fantuzzi, C.: A tank-based approach to impedance control with variable stiffness. In: Robotics and Automation (ICRA), 2013 IEEE International Conference on. pp. 4948–4953. IEEE (2013)
- Franchi, A., Secchi, C., Son, H.I., Bulthoff, H.H., Giordano, P.R.: Bilateral teleoperation of groups of mobile robots with time-varying topology. IEEE Transactions on Robotics 28(5), 1019–1033 (2012)
- 8. Franken, M., Stramigioli, S., Misra, S., Secchi, C., Macchelli, A.: Bilateral telemanipulation with time delays: A two-layer approach combining passivity and transparency. IEEE transactions on robotics **27**(4), 741–756 (2011)
- Hamaza, S., Georgilas, I., Richardson, T.: An adaptive-compliance manipulator for contactbased aerial applications. In: 2018 IEEE/ASME International Conference on Advanced Intelligent Mechatronics (AIM). pp. 730–735. IEEE (2018)
- Hamaza, S., Georgilas, I., Richardson, T.: Towards an adaptive-compliance aerial manipulator for contact-based interaction. In: 2018 IEEE/RSJ International Conference on Intelligent Robots and Systems (IROS). p. in press. IEEE (2018)
- Huber, F., Kondak, K., Krieger, K., Sommer, D., Schwarzbach, M., Laiacker, M., Kossyk, I., Parusel, S., Haddadin, S., Albu-Schaffer, A.: First analysis and experiments in aerial manipulation using fully actuated redundant robot arm. In: Intelligent Robots and Systems (IROS), 2013 IEEE/RSJ International Conference on. pp. 3452–3457. IEEE (2013)
- 12. Keemink, A.Q., Fumagalli, M., Stramigioli, S., Carloni, R.: Mechanical design of a manipulation system for unmanned aerial vehicles. In: Robotics and Automation (ICRA), 2012 IEEE International Conference on. pp. 3147–3152. IEEE (2012)

- 13. Mason, M.T.: Compliance and force control for computer controlled manipulators. IEEE Transactions on Systems, Man, and Cybernetics 11(6), 418–432 (1981)
- Mersha, A.Y., Stramigioli, S., Carloni, R.: Variable impedance control for aerial interaction. In: Intelligent Robots and Systems (IROS 2014), 2014 IEEE/RSJ International Conference on. pp. 3435–3440. IEEE (2014)
- 15. Michael, N., Fink, J., Kumar, V.: Cooperative manipulation and transportation with aerial robots. Autonomous Robots **30**(1), 73–86 (2011)
- Orsag, M., Korpela, C., Bogdan, S., Oh, P.: Valve turning using a dual-arm aerial manipulator. In: Unmanned Aircraft Systems (ICUAS), 2014 International Conference on. pp. 836–841. IEEE (2014)
- Pounds, P.E., Bersak, D.R., Dollar, A.M.: The yale aerial manipulator: grasping in flight. In: Robotics and Automation (ICRA), 2011 IEEE International Conference on. pp. 2974–2975. IEEE (2011)
- 18. Raibert, M.H., Craig, J.J.: Hybrid position/force control of manipulators. Journal of Dynamic Systems, Measurement, and Control **103**(2), 126–133 (1981)
- Ruggiero, F., Lippiello, V., Ollero, A.: Aerial manipulation: A literature review. IEEE Robotics and Automation Letters 3(3), 1957–1964 (2018)
- Salisbury, J.K.: Active stiffness control of a manipulator in cartesian coordinates. In: Decision and Control including the Symposium on Adaptive Processes, 1980 19th IEEE Conference on. vol. 19, pp. 95–100. IEEE (1980)
- 21. Secchi, C., Franchi, A., Bülthoff, H.H., Giordano, P.R.: Bilateral teleoperation of a group of uavs with communication delays and switching topology. In: Robotics and Automation (ICRA), 2012 IEEE International Conference on. pp. 4307–4314. IEEE (2012)
- 22. Siciliano, B., Villani, L.: Robot force control, vol. 540. Springer Science & Business Media (2012)
- 23. Spong, M.W.: Modeling and control of elastic joint robots. Journal of dynamic systems, measurement, and control **109**(4), 310–318 (1987)
- Suarez, A., Heredia, G., Ollero, A.: Lightweight compliant arm with compliant finger for aerial manipulation and inspection. In: Intelligent Robots and Systems (IROS), 2016 IEEE/RSJ International Conference on. pp. 4449–4454. IEEE (2016)